Reactions in the ^{8}B and ^{8}Li compound systems

Dean Halderson
Physics Department, Western Michigan University, Kalamazoo, Michigan 49008, USA
(Received 1 December 2005; published 28 February 2006)

Calculations are reported for reactions in the ^{8}B and ^{8}Li compound systems with the recoil corrected continuum shell model. Comparison with observed structure indicates that the spin-orbit component of the M3Y interaction must be modified near the middle of the p shell. Calculations are performed with three spin-orbit strengths. The prediction for ^{7}Be$(p,\gamma)^8$B, based on this model and available data, is that $S_{17}(0)$ equals 21.63 eV b and $S_{17}(20)$ 21.02 eV b. Calculations for ^{7}Li$(n,\gamma)^8$Li indicate that the ^{8}Li, 1_2^+ state is nearly degenerate with the 3^+ state. It is shown that a measurement of ^{7}Li$(n,\gamma)^8$Li(1_1^+) can locate the 0^+ state. It is also shown that ^{7}Be$(p,p')^7$Be$(1/2^-)$ can locate the 1^+ and 0^+ strength in ^{8}B.

DOI: 10.1103/PhysRevC.73.024612 PACS number(s): 24.10.−i, 21.60.−n, 25.40.Lw, 25.70.Ef

I. INTRODUCTION

The importance of the ^{7}Be$(p,\gamma)^8$B in solar processes is well known. Many references discuss the need for accurate, low-energy cross sections as a means of testing solar models and neutrino mixing. A good list of references to experimental articles may be found in Ref. [1] and for theoretical papers in Ref. [2]. However, the center of the Gamow window in ^{7}Be$(p,\gamma)^8$B is near 20 keV, whereas data have been limited to above 100 keV, and extrapolations must be made into the low-energy region. Hence, the mirror reaction, ^{7}Li$(n,\gamma)^8$Li, becomes important in gaining insight into and judging the appropriateness of these extrapolations. Such extrapolations require specific models, and the models should demonstrate their applicability to both systems.

Many models have been employed to extrapolate the ^{7}Be$(p,\gamma)^8$B cross section to zero energy. This article presents the results for ^{7}Be$(p,\gamma)^8$B and ^{7}Li$(n,\gamma)^8$Li as calculated with the recoil corrected continuum shell model (RCCSM) [3,4]. However, in addition to total capture cross sections, calculations are made for capture angular distributions and elastic and inelastic differential cross sections. The concern of this article is less for capture rates but more for the structure of these two compound systems that approach the proton and neutron drip lines. An understanding of these nuclei is essential before moving to other exotic systems.

The next section of this article describes the procedure for calculating low-energy capture calculations within the RCCSM. Section III discusses the structure of the ^{8}B and ^{8}Li systems and the necessity of modifying the spin-orbit component of the M3Y interaction [5]. It is demonstrated that the position of the first 0^+ state in both systems is extremely dependent on the strength of the spin-orbit interaction. Results are then described for capture, elastic, and inelastic scattering cross sections with three different spin-orbit strengths.

Although some features of the capture cross sections resemble previous calculations, the RCCSM provides a better spectrum and a more consistent description of the existing reaction data. The calculations are then used to predict the ^{8}B and ^{8}Li spectra above particle threshold. It is demonstrated that ^{7}Li$(n,\gamma)^8$Li(1^+) can locate the 0^+ state in ^{8}Li, and ^{7}Be$(p,p')^7$Be$(1/2^-)$ will locate the 0^+ and 1_2^+ strength in ^{8}B. Such measurements would add states to the spectrum of two nuclei for which very few states are known.

II. CAPTURE CALCULATIONS

The RCCSM provides coupled-channels solutions for bound and unbound wave functions. The wave functions are antisymmetric and contain no spurious components because the calculations are performed in the center-of-mass system. The input to the RCCSM is an oscillator size parameter, $\upsilon_0 = m\omega/\hbar$, the desired states of the $A-1$ core nuclei and realistic, translationally invariant interactions. Wave functions and scattering observables are calculated with R-matrix techniques. For p-shell nuclei [6] the channel wave functions within the channel radius, a_c, may be written as an expansion in a harmonic oscillator basis,

$$\Psi_{J_B} = \sum_{J_A\alpha\bar{l}\bar{j}\bar{n}\neq 0} f_{\bar{n}\bar{l}\bar{j}J_A\alpha J_B}[a^+_{\bar{n}\bar{l}\bar{j}}\otimes|\alpha J_A\rangle]^{J_B} + \sum_\beta d_\beta|\beta J_B\rangle, \quad (1)$$

where β runs over all $0\hbar\omega$, p-shell states with spin J_B, and $a^+_{\bar{n}\bar{l}\bar{j}}$ creates a particle in the core-nucleon, center-of-mass coordinate. The created particles are coupled to chosen p-shell states of the $A-1$ core, and the sum on n cannot include zero when $l=0$ or 1.

The translationally invariant, $E1$, $E2$, and $M1$ operators are given in the long-wavelength approximation by Ref. [7]

$$Q^{\rm eff}_{1q} = \sqrt{4\pi}\sum_i \bar{e}_i r_i Y_{lq}(\hat{r}_i), \quad (2)$$

where $\bar{e}/e = (\frac{N}{A}, -\frac{Z}{A})$ for (p,n),

$$Q^{\rm eff}_{2q} = \sqrt{4\pi/5}\sum_i \bar{e}_i r_i^2 Y_{2q}(\hat{r}_i) - e\sqrt{6}\frac{N}{A^2}\sum_{i<j}(\vec{r}_i\otimes\vec{r}_j)^2_q - e\sqrt{6}\frac{1}{A}\sum_{p<p'}(\vec{r}_p\otimes\vec{r}_{p'})^2_q + e\sqrt{6}\frac{1}{A}\sum_{n<n'}(\vec{r}_n\otimes\vec{r}'_n)^2_q, \quad (3)$$

where $\bar{e}/e = [\frac{A(A-2)+Z}{A^2}, \frac{Z}{A^2}]$ for (p,n), and p, p', n, n' count protons and neutrons, and

$$M_{10}+M'_{10} = \frac{e\hbar}{2mc}\left\{\sum_i(g_{l_i}l_z + g_{s_i}s_z) - \frac{N}{A^2}\sum_{i<j}[(\vec{r}_i\times\vec{p}_j)_z + (\vec{r}_j\times\vec{p}_i)_z] - \frac{1}{A}\sum_{p<p'}[(\vec{r}_p\times\vec{p}_{p'})_z + (\vec{r}_{p'}\times\vec{p}_p)_z] + \frac{1}{A}\sum_{n<n'}[(\vec{r}_n\times\vec{p}_{n'})_z + (\vec{r}_{n'}\times\vec{p}_n)_z]\right\}, \quad (4)$$

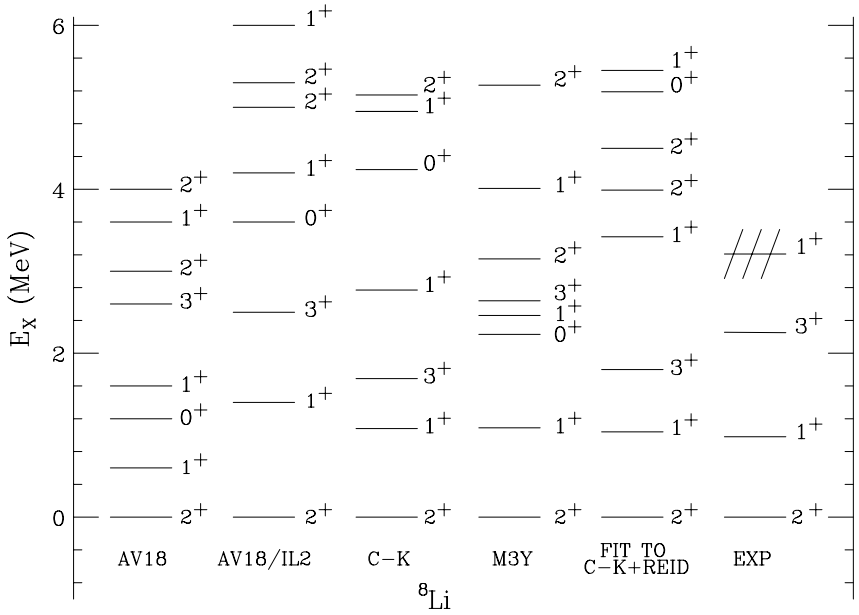

FIG. 1. ^{8}Li spectra with ground states set equal to zero.

where $g_{l_i} = \{[A(A-1)-N]/A^2, Z/A^2\}$ for (p,n) and $(\vec{r}_j \times \vec{p}_i)_z = (\vec{r}_j \otimes \vec{\nabla}_i)^1_0/\sqrt{2}$. Outside the channel radius, the two-body terms do not contribute and the three multipoles reduce to the customary single-particle operators used in Ref. [8], for example. However, in this work the spin of the target nucleons are allowed to contribute to M'_{10} as well as the spin of the incoming particle so that the $M1$ operator is the same at the boundary, a_c.

To implement the complete operators, their reduced matrix elements are calculated between the basis states $[a^+_{nlj}|J_A\rangle]^{J_B}$, where a^+_{nlj} creates a particle in the shell-model coordinate system and then the reduced matrix elements are transformed to the intrinsic coordinate system [3]. However, the expansion in Eq. (1) is only good within the channel radius, and one needs the reduced matrix elements calculated out to very large distances. Therefore, the matrix elements are first corrected by subtracting the contribution of the oscillators outside of a_c. For example, the reduced matrix elements of the $E1$ operator would receive the correction proportional to

$$\sum_{nn'} f^*_{nljJ_A\alpha J_B} f_{n'l'j'J'_A\alpha' J'_B} \int_{a_c}^{\infty} \langle \phi_{nlj} \| \sqrt{4\pi/3}\bar{e} Y_1(\hat{r}) r \| \phi_{n'l'j'} \rangle,$$

where the oscillators are calculated with a reduced $\upsilon = \upsilon_0(A-1)/A$. Outside the channel radius, the bound-state channel wave functions becomes properly normalized Whittaker functions, $N_{c'} W_{-\eta_{c'},l+1/2}(2k_{c'}r)/r$, and the continuum state for channel $c = ljJ_A\alpha J_B$ becomes $\Phi^{J_B}_c = \sum_{c'} (1/r) u^{J_B(+)}_{c'} |\alpha' J'_A l' j' J_B\rangle$, where $u^{J_B(+)}_{c'} = (\upsilon_c/\upsilon_{c'})(I_c\delta_{cc'} - O_c S_{cc'})$. Hence, one adds contributions for each open channel proportional to $\int_{a_c}^{\infty} W_{-\eta_c,l+1/2}(2k_b r) r [I_c(k_c r) - O_{c'}(k_{c'} r) S_{cc'}] dr$. One sees that the capture process divides nicely into an internal and external contribution in the R-matrix formalism.

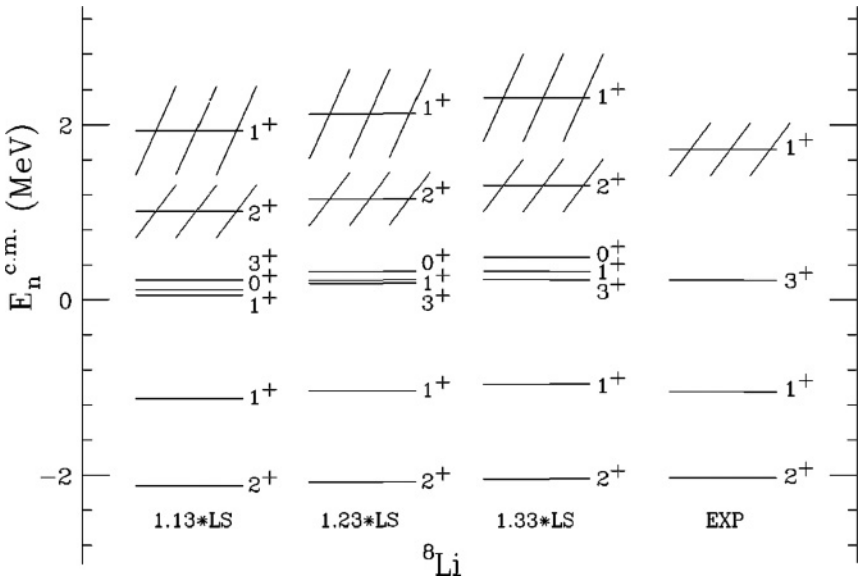

FIG. 2. ^{8}Li spectra measured from neutron threshold.

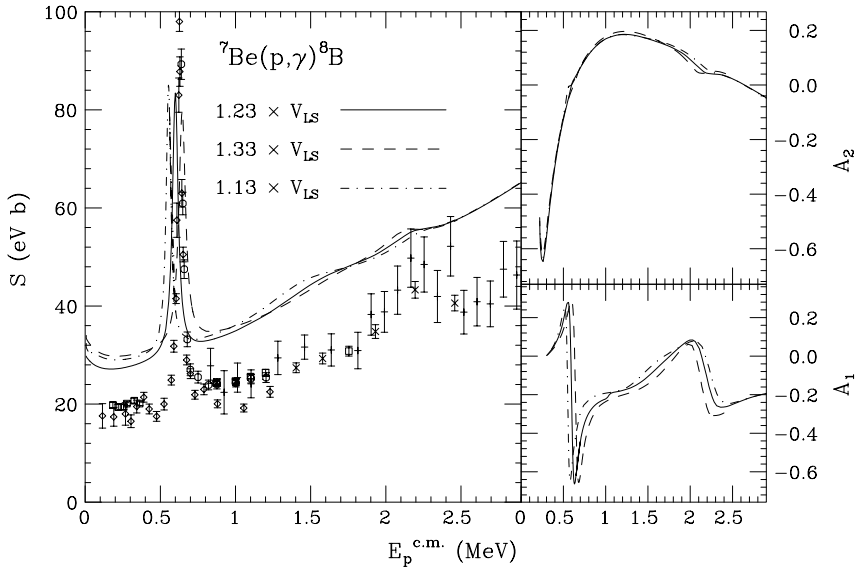

FIG. 3. ^{7}Be(p, γ)^{8}B S factor and angular distribution coefficients. Diamonds are data of Ref. [18]; crosses from Ref. [19]; circles, ×'s, and squares are BE1, BE2, and BE3S data of Ref. [1].

III. THE SPIN-ORBIT INTERACTION

From several calculations in the $A = 7$ systems [9,10], it was determined that the best predictions of continuum phenomena with the M3Y interaction were obtained when one includes only the $A - 1$ core states that are stable to single nucleon emission. This means including the $3/2^-$, $1/2^-$, and $7/2^-$ state of ^{7}Be for ^{8}B. The same three states have been included for ^{8}Li for consistency. These state were included in a previous calculation for ^{8}B in Ref. [11], where a slightly weakened, M3Y interaction provided good agreement with ^{7}Be + p elastic data [12]. However, when this same interaction was applied to ^{8}Li, it produced a bound 0^+ state below the known 3^+ state, which has not been observed.

At this point it is useful to look at two other calculations. The first is the Green's function Monte Carlo (GFMC) calculations of Ref. [13]. With just the AV18, two-body interaction, these authors also produce a 0^+ state far below the 3^+ for ^{8}Li. With the addition of the UIX three-body potential, this remains the case. However, when the IL-2, three-body interaction is employed, the levels reverse as shown in Fig. 1. It should be remembered that the three-body interaction is responsible for almost one-half of the splitting of the ^{15}N $1/2^-$ and $3/2^-$ states. So, to construct an equivalent two-body interaction, the spin-orbit component must be increased. The second calculation is a p-shell calculation for ^{8}Li with the Cohen and Kurath (6-16) interaction [14]. This is also shown in Fig. 1, where one sees

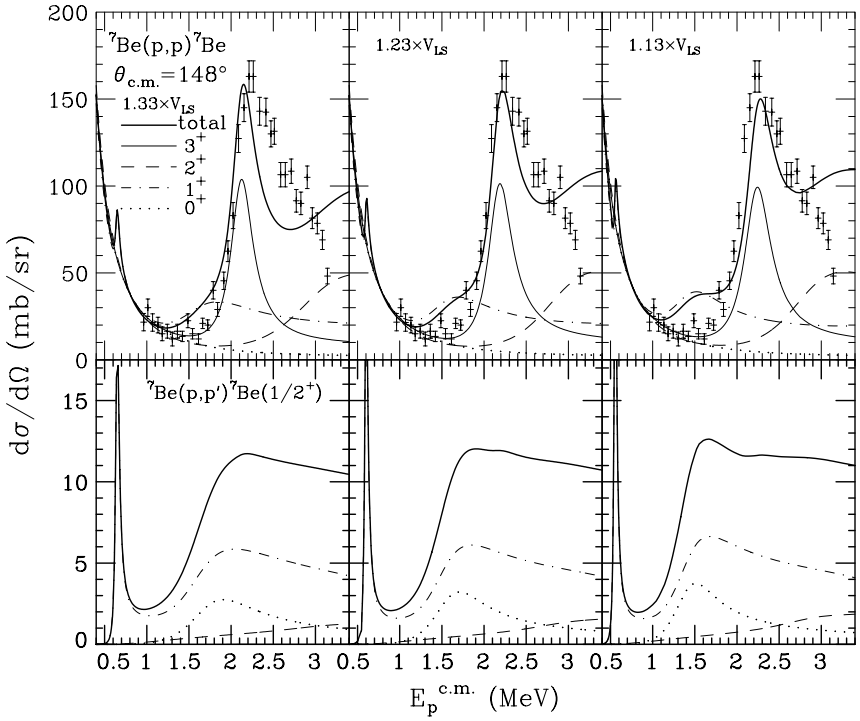

FIG. 4. Top panels are ^{7}Be(p, p)^{7}Be elastic excitation functions and bottom panels are ^{7}Be(p, p')^{7}Be($1/2^-$) inelastic excitation functions. Calculations for individual J^π include the Coulomb amplitude. Data are from Ref. [12].

a spectrum similar to AV18 + IL-2. The next calculation in Fig. 1 is the result of fitting two-body, Reid soft core [15] g-matrix elements up to $4\hbar\omega$, to the same sum of Yukawas used in M3Y, but with Cohen and Kurath matrix elements substituted where available. When analyzed, this interaction has a tensor component that is about one-half of M3Y and a spin-orbit component that is about 40% larger. By varying the strength of the spin-orbit components, one finds that the position of the 0^+ state is extremely sensitive it. The conclusion of this section is that the M3Y interaction, which provides agreement with almost all scattering data in the $A = 4$ compound system and reproduces the $p_{1/2} - p_{3/2}$ spin-orbit splitting in ^{5}He, must be modified to account for the three-body interaction that becomes important in the middle of the p shell. In the case of ^{8}Li, the most important modification is to the spin-orbit interaction.

IV. PROCEDURE AND RESULTS

The above fit to the Reid soft core and Cohen and Kurath matrix elements is used as a guide. The M3Y tensor interaction is multiplied by 0.7. This reduction of the tensor interaction is helpful throughout the p shell; however, although it has some effect on the 0^+, 3^+, and 1^+ level ordering, it has much less effect than the spin-orbit interaction. Therefore, calculations are made for three different spin-orbit strengths, 1.13, 1.23, and 1.33 times the M3Y component. One of these three factors should be appropriate for the middle of the p shell because they give a splitting of the ^{15}N $1/2^-$ and $3/2^-$ states of 4.2, 4.6, and 5.0 MeV, respectively, with υ_0= 0.312 fm^{-2}, whereas the unscaled value for M3Y is 3.7 and the experimental splitting is 6.3 MeV.

The M3Y interaction is supplemented by introducing the charge-symmetry breaking interaction of Ref. [16]. This is given by $V_{\rm CSB} = (V_\sigma m_\sigma^3/4\pi)Y(m_\sigma r) + \vec{\sigma}_1 \cdot \vec{\sigma}_2(V_\pi m_\pi^2/4\pi)Y(m_\pi r)$, where $V_\sigma = 65$ MeV fm^3, $V_\pi = 20$ MeV fm^3, and $Y(x) = e^{-x}/x$. Another supplement is the Skryme interaction [17] $V_S = t_3\delta(\vec{r}_1 - \vec{r}_2)\delta(\vec{r}_2 - \vec{r}_3)$. This original form of the Skryme interaction must be used, as opposed to the density-dependent form, because it is translationally invariant. The percentage of $V_{\rm CSB}$ and the strength, t_3, are adjusted for the different values of the spin-orbit strength so that the position of the 3^+ state in ^{8}Li corresponds closely to its position relative to the experimental neutron threshold, and the position of the ground state of ^{8}B corresponds closely to its position relative to the experimental proton threshold. Use of $V_{\rm CSB}$ accounts for the Okamoto-Nolan-Schiffer anomaly, and the Skryme interaction weakens the interaction in the interior. Table I shows the resulting values for the interaction strengths. A value of υ_0= 0.297 fm^{-2} is employed, and the oscillator expansion in Eq. (1) includes up to $2n + l = 16\hbar\omega$.

TABLE I. Potential strengths.

$\%V_{\rm LS}$	113	123	133
t_3(MeV fm^6)	1300	1620	1940
$\%V_{\rm CSB}$	62.5	57.1	51.7

The resulting spectrum for ^{8}Li is shown in Fig. 2, where one sees the 0^+ state moving to higher energies with increasing spin-orbit strength. One also sees that the $2_1^+ - 1_1^+ - 3^+$splitting is in good agreement with the experimental spectrum. The total capture cross section for ^{7}Be$(p, \gamma)^8$B and the two significant angular distribution coefficients from $d\sigma/d\Omega = A_0[1 + \sum_i A_i P_i(\cos\theta)]$ are shown in Fig. 3 for the three different spin-orbit strengths along with the data of Refs. [1,18,19]. From this figure and from Fig. 4, where the ^{7}Be$(p, p)^7$Be elastic excitation function is shown, one can see that the $2_1^+ - 1_1^+ - 3^+$splitting in ^{8}B is also in good agreement with experiment.

In this article two other capture calculations will be referenced. The first is the shell model embedded in the continuum (SMEC) calculation of Ref. [20] and the cluster calculation of Ref. [21]. Both of these calculations produce antisymmetric wave functions, however, of the two, only the cluster calculation removes spurious contributions from the scattering states by working with intrinsic coordinates as does the RCCSM. The applicability of the RCCSM, SMEC, and the cluster calculation depend on what phenomena one wishes to investigate.

The ^{7}Be$(p, \gamma)^8$B S factor in Fig. 3 looks very much like the equivalent S factor calculated with the cluster model, except that the contribution of the resonances was not shown in Ref. [21]. Near threshold the resonance contribution is small, and if one is only interested in extending the nonresonant cross section to low energies, then the $E1$ contribution is a good approximation. The nonresonant S factor is too large in both the RCCSM and the cluster calculation, however, in both works, one can see that the size depends on the interaction. In fact, it is possible to fit the data by altering the interaction; however,

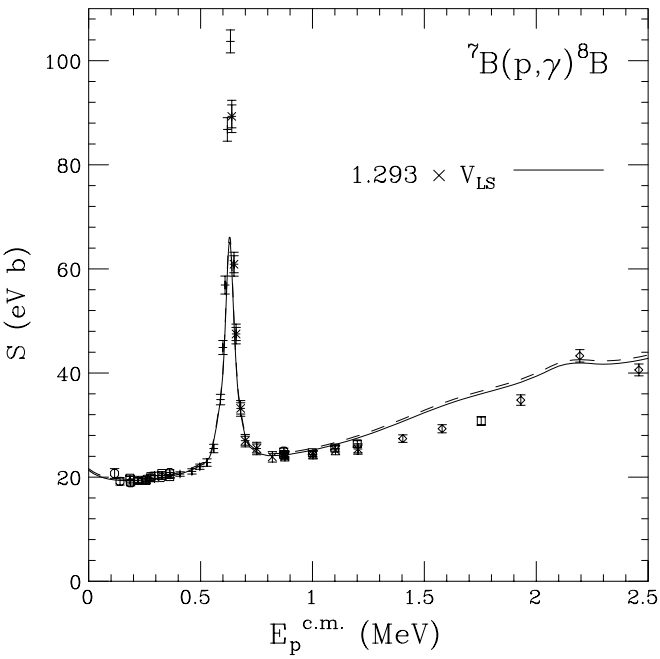

FIG. 5. S factor for ^{7}Be$(p, \gamma)^8$B. Line is 1.293 $\times V_{\rm LS}$ calculation with $E1$ contribution scaled by 0.726. Circles, $\times$'s, squares, and diamonds are BE3L, BE1, BE3S, and BE2 data from Ref. [1].

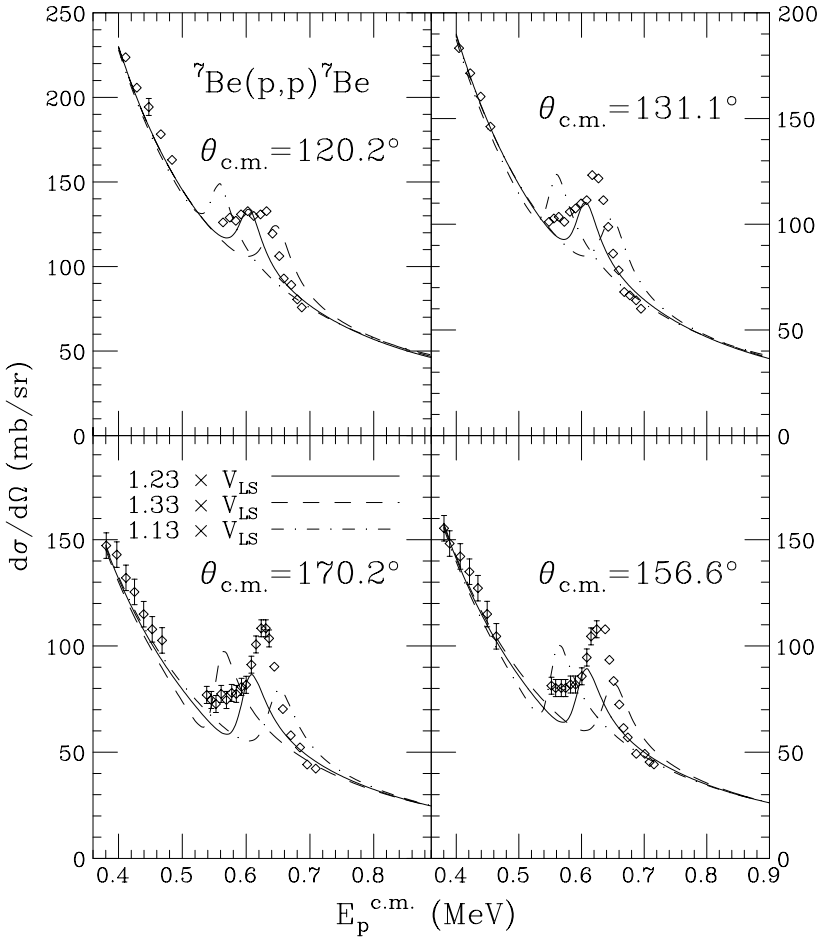

FIG. 6. Elastic ^{7}Be(p, p)^{7}Be. Data are from Ref. [25]. Lines are RCCSM calculations.

one then changes the spectrum. In Ref. [21] the overestimate of the nonresonant S factor is explained by the limited basis used to calculate the bound states. This effect was seen in an RCCSM calculation for $^3H(p, \gamma)^4$He [22]. Here it was found that the cross section, determined from a $6\hbar\omega$ calculation of ^{3}H and ^{3}He, was 12% smaller than that determined from a $0\hbar\omega$ calculation of ^{3}H and ^{3}He, but only when Q_{1q}^{eff} was used for the $E1$ operator. The cross section actually increased for the larger $\hbar\omega$ when the current $E1$ operator was employed, leading to better conservation of current. In the SMEC calculation the magnitude of the nonresonant contribution agrees with the data. This is possible because the SMEC has the flexibility of choosing an interaction that provides the continuum coupling that is different than that used to produce the structure and of choosing a particle-core, single-particle potential. The choice that reproduced the nonresonant strength leads to a resonant strength that is far too small.

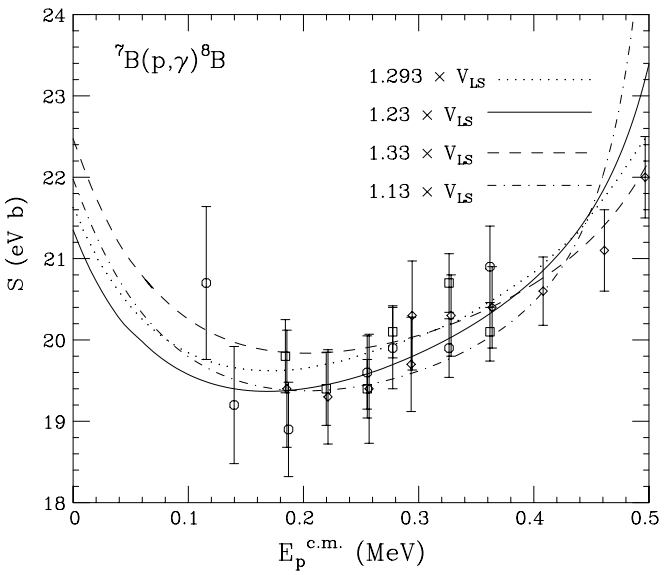

FIG. 7. Low energy S factor for ^{7}Be(p, γ)^{8}B. Lines are RCCSM calculations with scaled $E1$ contributions. Squares, diamonds, and circles are BE3S, BE1, and BE3L data from Ref. [1].

By scaling the nonresonant S factor of calculated in the cluster calculation of Ref. [23], the authors of Ref. [1] obtained a good fit to their data and then predict the S factor for the ^{7}Be(p, γ)^{8}B at $E_p^{\text{c.m.}} = 20$ keV [$S_{17}(20)$] and $E_p^{\text{c.m.}} =$ zero [$S_{17}(0)$]. One can do the same with the RCCSM result. A spin-orbit strength of $1.293 \times V_{\text{LS}}$ places the 1^+ resonance at its observed position, and multiplying the $E1$ strength by 0.726 yields the S factor shown in Fig. 5. This figure shows that the 1^+ resonance strength is one-third too small. This is consistent with the transition rate for $1^+ \rightarrow 2^+$ in ^{8}Li where the calculated $B(M1)$ is 2.09, 2.03, and 2.06 W.u. for $1.33 \times V_{\text{LS}}$, $1.23 \times V_{\text{LS}}$, and $1.13 \times V_{\text{LS}}$, respectively, whereas the experimental value is 2.8 ± 0.9 W.u. [24]. This is also consistent with the

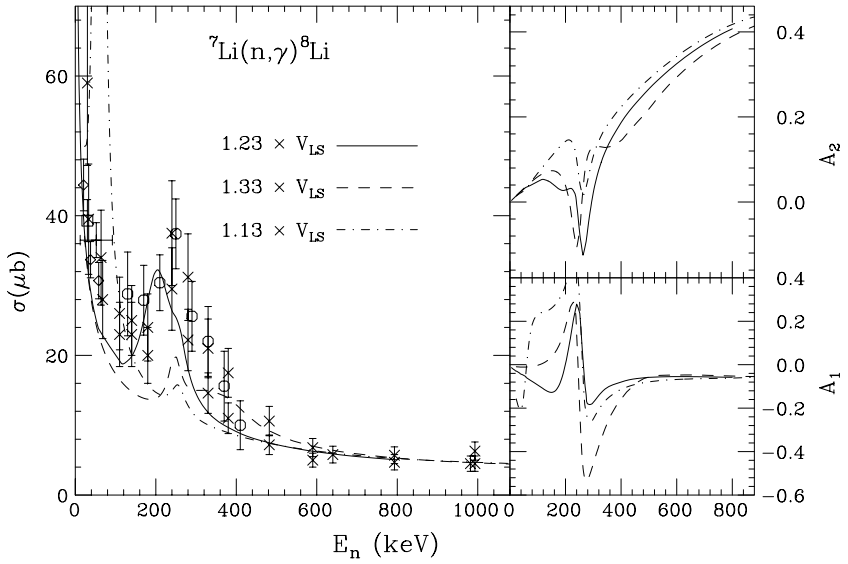

FIG. 8. Capture cross section and angular distribution coefficients for ^{7}Li$(n, \gamma)^8$Li. Diamonds are capture to the ground state only and are from Ref. [26]. Cross, circles, square, and ×'s are total cross sections from Refs. [27–30]. Lines are calculations for capture to the ground state.

^{7}Be$(p, p)^7$Be excitation functions shown in Fig. 6. Here the calculated resonance has only about one-half the experimental strength of Ref. [25].

Figure 7 displays the low energy region of Fig. 5 and also the results for scaling the $1.33 \times V_{\rm LS}$, $1.23 \times V_{\rm LS}$, and $1.13 \times V_{\rm LS}$, calculations. The fitted curve depends on which of the data sets from Ref. [1] one includes. This adds an uncertainty that was extracted in Ref. [1] by examining the data and also using the results of scaling various calculations. The final result for $S_{17}(0)$ from Ref. [1] is 22.1 ± 0.6(expt) $\pm$ 0.6(theor) eV b. In this work all data from Ref. [1] below 0.5 MeV were included in a fit. From Fig. 7 the RCCSM result for the $1.293 \times V_{\rm LS}$ calculation is $S_{17}(0)$ equals 21.63 eV b. Also, $S_{17}(20)$ is predicted to 21.02 eV b with the same experimental uncertainties derived in Ref. [1].

Shown in Fig. 8 is the ^{7}Li$(n, \gamma)^8$Li cross section along with data of Refs. [26–30] Data of Ref. [28] have been corrected as suggested in Ref. [27]. The data of Ref. [26] includes only capture to the ground state, whereas the other data include capture to both the ground and first excited states. The calculation is only for capture to the ground state. One notes two features in this figure. First, the nonresonant contribution of the calculation does not need a scale factor, just as in the cluster calculation of Ref. [21]. Nonresonant capture to the first excited state is only about 10% that of capture to the ground state, as shown in Fig. 9, so this would make little difference. Therefore, nonresonant capture for ^{8}B must be reduced by 0.726, whereas no factor is needed for ^{8}Li, given the present data sets. No explanation for this is offered in this article.

Second, one notes that the peak of the resonance is at the position of the 1^+ state and not the 3^+ state. This is most obvious in the $1.13 \times V_{\rm LS}$, calculation where the 1^+ state comes just above threshold and gives a very large cross section. The dominance of the 1^+ state is confirmed in bound-state shell-model calculations where the $B(M1)$ for the $1_2^+ \rightarrow 2^+$ transition is 0.86, 0.92, and 1.58 W.u. for $1.33 \times V_{\rm LS}$, $1.23 \times V_{\rm LS}$, and $1.13 \times V_{\rm LS}$, respectively, and 1.49 W.u. for Cohen and Kurath (6-16), whereas the $3^+ \rightarrow 2^+$ gives 0.06,

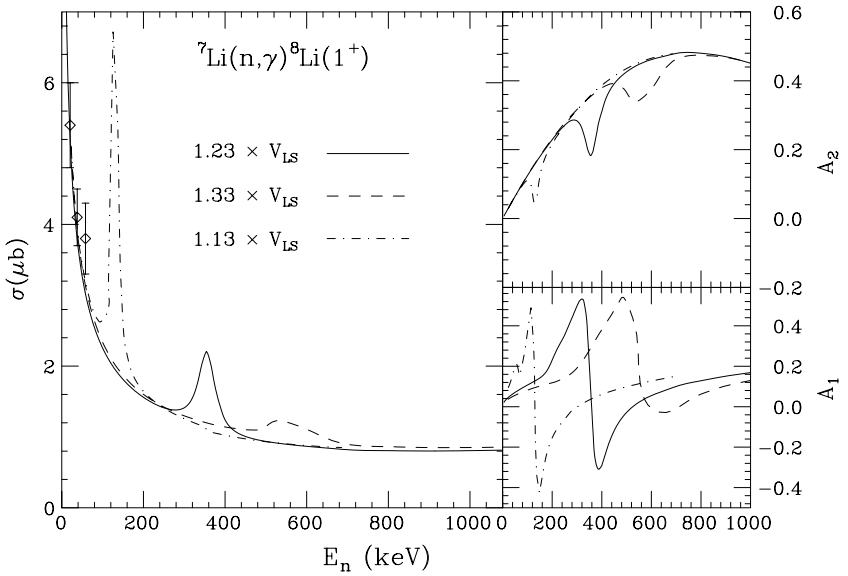

FIG. 9. Capture cross section and angular distribution coefficients for ^{7}Li$(n, \gamma)^8$Li (1^+). Data are from Ref. [26]. Lines are RCCSM calculations.

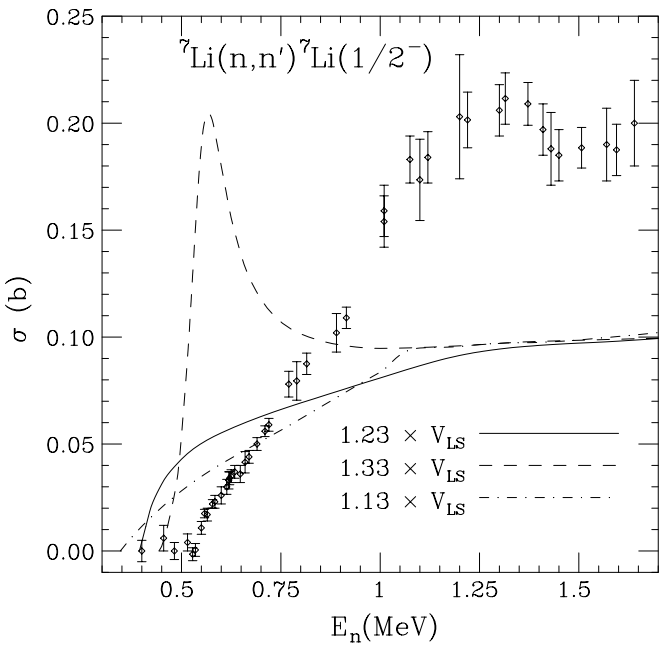

FIG. 10. The cross section ^{7}Li$(n, n')^7$Li$(1/2^-)$. Data are from Ref. [31]. Lines are RCCSM calculations.

0.05, 0.04, and 0.23 W.u. The calculation indicates that the 3^+ state needs the near-degenerate 1^+ state to reproduce the observed strength. The calculation also indicates that it is the 1^+_3 state that appears in the experimental spectrum of Fig. 2. The state appearing in the experimental spectrum is seen in ^{7}Li$(n, n')^7$Li$(1/2^-)$, [31], and, although coming too high in energy, the calculated 1^+_3 state has a large reduced width in that channel. Additional evidence that the 1^+_2 state is close to the 3^+ state comes from Fig. 4. The 3^+ strength extracted from an *R*-matrix fit to data [12] looks almost exactly like that of the RCCSM calculation. Therefore, additional strength is in this region, and the calculation predicts that this can only be 1^+ strength.

The ^{7}Li$(n, \gamma)^8$Li(1^+) cross section is shown in Fig 9 with the data of Ref. [26]. The resonance structure in this cross section is because of the 0^+ state. If the experiments can be extended to higher energies, then the 0^+ state can be located. Additional evidence that the 0^+ state lies between the ^{7}Li$(3/2^-)+n$ and ^{7}Li$(1/2^-)+n$ threshold is shown in Fig. 10. If the 0^+ state lies above the inelastic threshold, it would show strongly in the ^{7}Li$(n, n')^7$Li$(1/2^-)$ cross section as in the $1.33 \times V_{LS}$ calculation.

Finally, a way to test the presence of 0^+ and 1^+ strength near the 3^+ state is demonstrated in the bottom panels of Fig. 4. This strength is the only strength in this region in ^{7}Be$(p, p')^7$Be$(1/2^-)$. This experiment is recommended as the first experiment in the pursuit of additional states in ^{8}B and ^{8}Li. It is likely that the experiment would yield a cross section that is somewhat smaller than predicted, based on the contribution of the inelastic channel to the width of the 1^+ state. One can see in Fig. 5 that the calculated width is about 50 keV, whereas the analysis of the experiment yielded 35.7 $\pm$ 0.6 keV. However, only four or five data points would be required to see the rise in strength, and the experiment of Ref. [12] has shown that cross sections of this magnitude can be measured.

V. CONCLUSION

This article has presented the RCCSM calculations for reactions in the ^{8}B and ^{8}Li compound systems. Calculations employed the M3Y interaction with a reduced tensor component and three different spin-orbit strengths. The resulting ^{7}Be$(p, \gamma)^8$B nonresonant *S*-factor resembles previous calculations, while the spectrum and the resonant contributions provide better agreement with experimental results. The prediction based on this model and available data is that $S_{17}(0)$ equals 21.63 eV b and $S_{17}(20)$ 21.024 eV b.

Calculations for ^{7}Li$(n, \gamma)^8$Li indicated that the 3^+ state does not have enough strength to reproduce that which is observed, and, therefore, the ^{8}Li 1^+_2 state should be nearly degenerate with the 3^+ state. It was shown that a measurement of ^{7}Li$(n, \gamma)^8$Li(1^+_1) can locate the 0^+ state, and that it is most likely between the elastic and first inelastic neutron thresholds. It is also shown that ^{7}Be$(p, p')^7$Be$(1/2^-)$ can locate the 1^+ and 0^+ strength in ^{8}B, and that this cross section is large enough to be measured with existing experimental setups.

ACKNOWLEDGMENT

This work was supported by National Science Foundation grant PHY-0456943.

[1] A. R. Junghans, E. C. Mohrmann, K. A. Snover, T. D. Steiger, E. G. Adelberger, J. M. Casandjian, H. E. Swanson, L. Buchmann, S. H. Park, A. Zyuzin, and A. Laird, Phys. Rev. C **68**, 065803 (2003).
[2] B. K. Jennings, S. Karataglidis, and T. D. Shoppa, Phys. Rev. C **58**, 3711 (1998).
[3] R. J. Philpott, Nucl. Phys. **A289**, 109 (1977).
[4] D. Halderson, Int. J. Mod. Phys. E **14**, 171 (2005).
[5] G. Bertsch, J. Borysowicz, H. McManus, and W. G. Love, Nucl. Phys. **A284**, 399 (1977), the interaction described on p. 412.
[6] D. Halderson, Nucl. Phys. **A707**, 65 (2002).
[7] H. J. Rose and D. M. Brink, Rev. Mod. Phys. **39**, 306 (1967).
[8] R. F. Christy and I. Duck, Nucl. Phys. **24**, 89 (1961).
[9] D. Halderson, Nucl. Phys. **A707**, 65 (2002).
[10] D. Halderson, Phys. Rev. C **70**, 041603(R) (2004).
[11] D. Halderson, Phys. Rev. C **69**, 014609 (2004).
[12] G. V. Rogachev *et al.*, Phys. Rev. C **64**, 061601(R) (2001).
[13] S. C. Pieper, R. B. Wiringa, and J. Carlson, Phys. Rev. C **70**, 054325 (2004).
[14] S. Cohen and D. Kurath, Nucl. Phys. **73**, 1 (1965).
[15] R. V. Reid, Jr., Ann. Phys. **50**, 411 (1968).
[16] S. Shlomo, Rep. Prog. Phys. **41**, 957 (1978).
[17] T. H. R. Skyrme, Nucl. Phys. **A9**, 615 (1959).

[18] B. W. Filippone, A. J. Elwyn, C. N. Davids, and D. D. Koetke, Phys. Rev. C **28**, 2222 (1983).
[19] F. J. Vaughn, R. A. Chalmers, D. Kohler, and L. F. Chase, Phys. Rev. C **2**, 1657 (1970).
[20] K. Bennaceur, F. Nowacki, J. Okołowicz, and N. Płoszajczak, Nucl. Phys. **A651**, 289 (1999).
[21] P. Descouvemont, Phys. Rev. C **70**, 065802 (2004).
[22] D. Halderson, Phys. Rev. C **70**, 034607 (2004).
[23] P. Descouvemont and D. Baye, Nucl. Phys. **A567**, 341 (1994).
[24] D. R. Tilley, J. H. Kelley, J. L. Godwin, D. J. Millener, J. E. Purcell, C. G. Sheu, and H. R. Weller, Nucl. Phys. **A745**, 155 (2004).
[25] C. Angulo *et al*., Nucl. Phys. **A716**, 211 (2003).
[26] Y. Nagai, M. Igashira, T. Takaoka, T. Kikuchi, T. Shima, A. Tomyo, A. Mengoni, and T. Otsuka, Phys. Rev. C **71**, 055803 (2005).
[27] M. Heil, F. Kaeppeler, M. Weischer, and A. Mengoni, Astrophys. J. **507**, 997 (1998).
[28] M. Weischer, R. Steininger, and F. Kaeppeler, Astrophys. J. **344**, 464 (1989).
[29] Y. Nagai *et al*., Astrophys. J. **381**, 444 (1991).
[30] W. L. Imhof *et al*., Phys. Rev. **114**, 1037 (1959).
[31] J. M. Freeman, A. M. Lane, and B. Rose, Phil Mag. **46**, 17 (1955).